Available online at www.eccomasproceedia.org
Eccomas Proceedia COMPDYN (2017) 4342-4357

ECCOMAS
Proceedia

COMPDYN 2017
6th ECCOMAS Thematic Conference on
Computational Methods in Structural Dynamics and Earthquake Engineering
M. Papadrakakis, M. Fragiadakis (eds.)
Rhodes Island, Greece, 15–17 June 2017

RESIDUAL LOAD CAPACITY OF FIRE-DAMAGED RUBBER BEARINGS FOR R.C. BASE-ISOLATED BUILDINGS SUBJECTED TO NEAR-FAULT EARTHQUAKES

F. Mazza[1] **and F. Alesina**[2]

[1] Dipartimento di Ingegneria Civile, Università della Calabria
Via P. Bucci, 87036 Rende (CS), Italy
e-mail: fabio.mazza@unical.it

[2] Dipartimento di Ingegneria Civile, Università della Calabria
Via P. Bucci, 87036 Rende (CS), Italy
fabio.alesina@unical.it

Keywords: R.C. Base-isolated Framed Structure; Fire-Damaged Rubber and Lead-Rubber Bearings; Nonlinear Incremental Dynamic Analysis; Near- and Far-Fault earthquakes.

Abstract. *A base-isolation system of framed buildings frequently involves elastomeric materials (e.g. High-Damping-Laminated-Rubber Bearings, HDLRBs, and Lead-Rubber Bearings, LRBs), which are susceptible to deterioration when fire occurs. On the other hand, fire-damaged HDLRBs and LRBs may elongate the fundamental vibration period of a base-isolated building, shifting it into the resonant region under the long-duration horizontal pulses of near-fault ground motions. To study the nonlinear seismic response following fire in HDLRBs and LRBs, a numerical investigation is carried out on six-storey r.c. base-isolated buildings comprising a basement and five storeys above ground. Three fire scenarios are considered, with the fire compartment confined to the area of the base-isolated level (i.e. F0), first level of the superstructure (i.e. F1) and both levels (i.e. F0/1). Base-isolated structures in a no fire situation are compared with those in the event of fire, at different durations of fire resistance for the basement (i.e. R30) and the superstructure (i.e. R60). Different values of the opening factor are assumed in the basement so as to obtain the R30 fire resistance with different fire temperatures for HDLRBs and LRBs. To this end, transient analysis corresponding to the EC1 time-temperature curves in the basement is carried out by means of a finite element modelling of HDLRBs and LRBs. A reduction of the mechanical properties of the fire-damaged isolators is evaluated in line with a 200°C isotherm method. Reduced mechanical properties of r.c. cross-sections are considered by means of a thermal-mechanical mapping analysis, in line with the 500°C isotherm method proposed by Eurocode 2. A nonlinear incremental dynamic analysis of the base-isolated structures is carried out considering near- and far-fault earthquakes. The nonlinear seismic analysis uses a lumped plasticity model to describe the inelastic behaviour of the r.c. frame members; the response of an HDLRB is simulated with a viscoelastic model, with variable stiffness properties in the horizontal and vertical directions, while a bilinear model is considered for an LRB.*

Peer-review under responsibility of the organizing committee of COMPDYN 2017.
doi: 10.7712/120117.5728.17323

1 INTRODUCTION

Thanks to major improvements of seismic codes and guidelines, considerable advances in the application of base-isolation technique have been accomplished in recent years in the area of seismic protection of structures. Thus, fire in a base-isolated structure following a seismic event is not uncommon making the structure more vulnerable to aftershocks, because it will experience an earthquake without any retrofit. Given the extensive use of reinforced concrete (r.c.) for the superstructure and elastomeric materials (e.g. High-Damping-Laminated-Rubber Bearings, HDLRBs, and Lead-Rubber Bearings, LRBs) for the bearings, it is necessary to fully understand the effect of fire on their seismic resistance. Under high temperatures, r.c. frame members undergo degradation of material properties [1], weakening steel reinforcement and concrete, stiffness [2, 3], produced by spalling of concrete on the sides exposed to fire, and ultimate ductility [4, 5], with a reduction in the frame members exposed to fire on three and four sides and an increase on the bottom side of beams due to fire-reduced yield strength of the longitudinal bars in tension. Moreover, mechanical and geometrical properties of HDLRBs and LRBs are reduced when temperatures exceed the point at which vulcanization between layers of rubber and steel plates occurs [6]. However, there is a high degree of uncertainty about the residual seismic load capacity of fire-damaged isolators and r.c. frame members, so a lack of in-depth knowledge to decide whether strengthening of the superstructure and replacement of the base-isolation system are necessary. This paper contributes toward a solution of this problem, by providing outcomes on how a base-isolated building damaged by fire would perform during near- and far-fault seismic aftershocks.

A numerical study is presented to investigate the nonlinear seismic response following fire of a six-storey r.c. base-isolated building, composed of a basement and five storeys above ground, designed in a high-risk seismic zone in accordance with the current Italian code [7]. The base-isolation system consists of HDLRBs and LRBs, inserted at the top of the columns of the basement, designed on the basis of different values of the fundamental vibration periods and equivalent viscous damping ratios in order to obtain the same value of the spectral acceleration. Three fire scenarios are considered, with the fire compartment confined to the area of the base-isolated level (i.e. F0), first level of the superstructure (i.e. F1) and both levels (i.e. F0/1). For each scenario, parametric temperature-time curves are evaluated in accordance with Eurocode 1 [8], with different values of the opening factor representing the amount of ventilation. Specifically, R30 fire resistance is obtained in the basement when assuming two fire temperatures for HDLRBs (i.e. T=300°C and 400°C) and LRBs (i.e. 250°C and 300°C) while R60 fire resistance in the superstructure is related to T=800°C. Reduction factors of the horizontal and vertical stiffnesses of the HDLRBs and LRBs, due to the fire-damaged cross-section, are considered in line with a proposed 200°C isotherm method. To this end, transient response, obtained by means of a finite element modelling of the bearings implemented in the computer program ABAQUS [9]. Reduced mechanical properties of r.c. cross-sections of beams and columns are also assumed in accordance with the 500°C isotherm provided by Eurocode 2 [10]. Nonlinear incremental dynamic analysis of the test structures is carried out by considering two sets of records scaled on the design hypotheses: i.e. NFE set, consisting of seven near-fault earthquakes, with significant horizontal pulses, selected from the Pacific Earthquake Engineering Research center database [11]; FFE set, consisting of seven far-fault records derived from the European Strong Motion database [12].

2 BASE-ISOLATED TEST STRUCTURES

A six-storey r.c. base-isolated (BI) office building with symmetric plan (Figure 1a), composed of a basement and five storeys above ground (Figure 1b), is the test structure chosen for the numerical investigation. Specifically, two base-isolation systems are considered, consisting of fifteen identical HDLRBs and LRBs inserted on the top of the columns of the basement. A grid of rigid beams is placed at the base of the superstructure on the isolators, while rigid columns are placed in the basement below the isolators. Dead and live gravity loads used in the design are assumed equal to: 6.1 kN/m^2 and 3 kN/m^2, for the isolated floor; 4.4 kN/m^2 and 3 kN/m^2, for the top floor; 5.7 kN/m^2 and 3 kN/m^2, for the other floors. Then, perimeter masonry infills are taken into account considering a gravity load of 2.7 kN/m^2 along the perimeter. A cylindrical compressive strength of 25 N/mm^2 for the concrete and a yield strength of 450 N/mm^2 for the steel are assumed for the r.c. frame members. Seismic loads are evaluated in line with the Italian code (NTC08, [7]), assuming: high-risk seismic zone (peak ground acceleration in the horizontal direction, PGA_H=0.283g and 0.345g, at the life-safety (LS) and collapse-prevention (CP) limit states, respectively); elastic response of the superstructure (behaviour factor, q_H=1.0); medium-dense subsoil type (class C, with subsoil parameter S_H=1.41 and 1.31 at the LS and CP limit states, respectively).

Base-isolated structures are designed for the same value of spectral acceleration at the LS limit state (i.e. S_a=0.09g) and nominal stiffness ratio of the isolation system (i.e. $\alpha_{K0}=K_{V0}/K_{H0}$ =1770, being K_{V0} and K_{H0} the vertical and horizontal nominal stiffnesses). To this end, different values of the fundamental vibration period (i.e. $T_{I,H}$=2.84s and 2.5s) and equivalent viscous damping ratio (i.e. $\xi_{I,H}$=10% and 20%) are assumed in the horizontal direction for the HDLRBs and LRBs, respectively. Moreover, the vibration periods with prevailing component in the vertical direction (i.e. $T_{I,V}$=0.067s, for HDLRBs, and 0.059s, for LRBs) correspond to the same value of the equivalent viscous damping ratio in the same direction (i.e. $\xi_{I,V}$=5%).

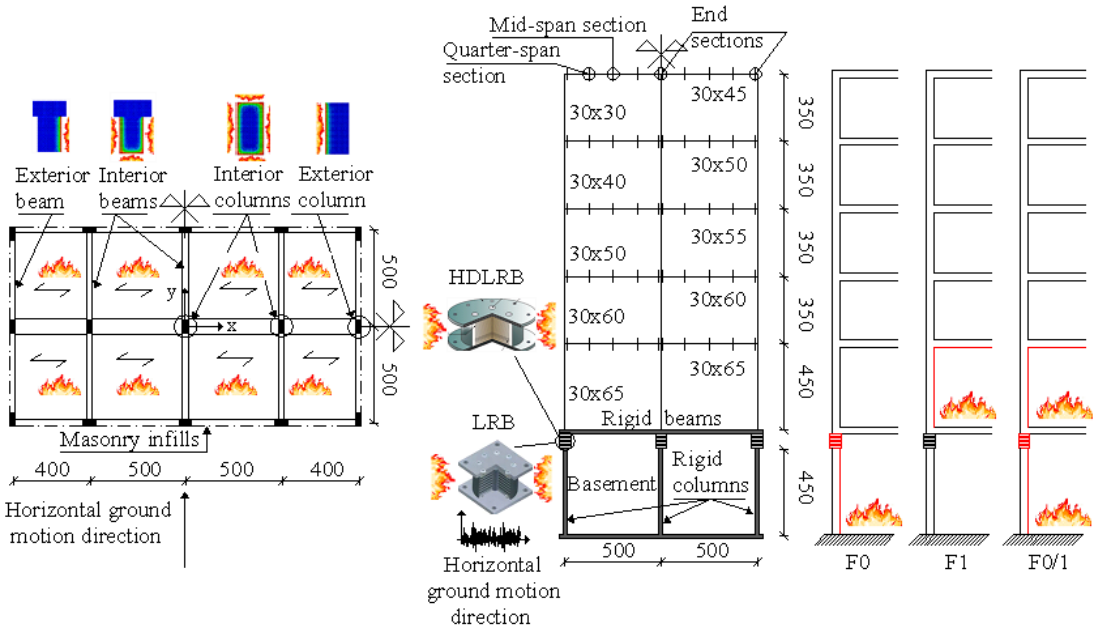

(a) In-plan fire scenario and fire-damaged r.c. frame members.

(b) In-elevation fire scenarios and fire-damaged HDLRBs and LRBs.

Figure 1: Base-isolated test structure (unit in cm).

Different values of the isolation ratio α_I, defined as the ratio between the fundamental vibration period of base-isolated structure ($T_{I,H}$) and fixed-base structure above the isolation

system ($T_{F,x}$ and $T_{F,y}$), are obtained for HDLRBs, $\alpha_{I,x}$=3.69 and $\alpha_{I,y}$=4.0, and LRBs, $\alpha_{I,x}$=3.25 and $\alpha_{I,y}\cong$3.52, along the principal in-plan directions. The design of the superstructure complies with the LS limit state, satisfying minimum conditions for the longitudinal bars of the r.c. frame members according to the provisions for low ductility class imposed by NTC08 [7]. The length and cross-sections of the r.c. frame members are also shown in Figure 1. Further details can be found in previous works by the author [13, 14].

The design of the HDLRBs and LRBs fulfill the CP limit state checks: i.e. $\gamma_{tot}=\gamma_s+\gamma_c+\gamma_\alpha\leq 5$ and $\gamma_s\leq 2$, where γ_{tot} represents the total design shear strain, while γ_s, γ_c and γ_α represent the shear strains of the elastomer due to seismic displacement, axial compression and angular rotation, respectively; $(P_{cr}/P)_{min}\geq 2$, where P and P_{cr} represent the maximum compression axial load and the corresponding critical buckling load; $|\sigma_t/\sigma_{tu}|_{max}\leq\min(2G,1MPa)$, σ_t being the minimum tensile stress and σ_{tu} the corresponding ultimate value. The following mechanical properties of the HDLRB and LRB are reported in Table 1: G and E_b, shear and volumetric compression moduli of the elastomer; G_p and E_p, shear and elastic moduli of the lead; τ_{py}, yield stress of the lead. It should be noted that the lead core is neglected in the calculation of the critical buckling load for LRBs [15]; design values of P_{cr} and displacement at the collapse prevention limit state (d_{dC}) are also reported in Table 1.

Type	*G*	E_b	G_p	E_p	τ_{py}	P_{cr}	d_{dC}
HDLRB	0.35	2000	-	-	-	3359	0.289
LRB	0.43	2000	130	16000	10.5	3008	0.220

Table 1: Mechanical and design parameters of the base-isolation systems (units in MPa, kN and m).

In Table 2 initial stiffnesses (i.e. K_{H0} and K_{V0}) and corresponding equivalent damping coefficients (i.e. C_H and C_V) of the HDLRBs and LRBs are reported together with the following geometrical properties: the diameter of the elastomer (D_e) and that of the lead core (D_l); the total thickness of elastomer (t_e); primary (S_1) and secondary (S_2) shape factors. Usually, the lead plug has a diameter about 1/7 times that of the outer diameter of the rubber. Note that the design of the isolators depends on the condition imposed on the maximum value of the total shear strain (γ_{tot}), while no tensile forces are found in the isolators.

Type	K_{H0}	K_{V0}	C_H	C_V	D_e	D_l	t_e	S_1	S_2
HDLRB	6360	11263000	574	12070	0.538	-	0.187	22.4	2.9
LRB	8190	14487500	1303	13685	0.428	0.064	0.153	26.1	2.8

Table 2: Geometrical and design parameters of the base-isolation systems (units in kN, m and s).

3 FIRE-DAMAGE IN THE SUPERSTRUCTURE AND ISOLATORS

Three fire scenarios with uniform temperature within the fire compartment are considered, assuming fire confined to the whole area (Figure 1a) of the lower levels in the base-isolated test structures (Figure 1b): i.e. base-isolated level (i.e. F0), first level of the superstructure (i.e. F1) and both levels (i.e. F0/1). On ther hand, HDLRBs and LRBs of the basement, in the F0 and F0/1 scenarios, are exposed to fire on all lateral surfaces (Figure 1b), hypothesizing a seismic gap around the building which allows the base-isolation horizontal movement during an earthquake. To simulate the time-temperature evolution, during the heating and cooling phases of an actual fire, the EC1 natural fire curves [8] are considered

$$\theta_g = 20+1325\left(1-0.324e^{-0.2t^*}-0.204e^{-1.7t^*}-0.472e^{-19t^*}\right) \quad (1a)$$

$$\theta_g = \theta_{\max}-250\left(3-t^*_{\max}\right)\left(t^*-t^*_{\max}\right) \quad (1b)$$

where t^* is a fictitious time obtained considering the time t (in hours) multiplied by a dimensionless parameter equal to

$$\Gamma = \left(O/b\right)^2 \Big/ \left(0.04/1160\right)^2 \tag{1}$$

function of the opening factor (O) and thermal absorptivity (b) of surrounding surfaces of the compartment. Moreover, t^*_{max} corresponds to the maximum temperature θ_{max} in the heating phase which lasts

$$t^*_{\max} = \left(0.2 \cdot 10^{-3} q_{t,d} / O\right) \Gamma \tag{3}$$

being the total design fire load density

$$q_{t,d} = q_{f,d} \, A_f / A_t \tag{4}$$

related to the total area of the compartment (A_t) and the floor value ($q_{f,d}$) corresponding to the surface area of the floor (A_f). Table 3 reports the aforementioned design parameters of fire load in the case of the F1 (i.e. superstructure) and F0 (i.e. basement) fire scenarios assuming 60 min (i.e. R60) and 30 min (i.e. R30) of exposure, respectively. Note that a temperature of about 800°C corresponds to R60 fire resistance in the superstructure. Different values of the opening factor are considered in the basement so as to obtain the same fire resistance (i.e. R30) when assuming two fire temperatures for HDLRBs (i.e. T=300°C and 400°C) and LRBs (i.e. 250°C and 300°C). Finally, the F0/1 fire scenario is derived from F0 and F1, which occur simultaneously. Further details on fire modelling can be found in [14].

Fire resistance (min)	*Fire scenario*	*T (°C)*	$q_{f,d}$ *(MJ/m²)*	A_f *(m²)*	A_t *(m²)*	*O* $(m^{1/2})$	*b* $(J/m^2s^{1/2}K)$
R30	F0 (HDLRB)	300	445	180	612	0.0094	1100
		400				0.0114	
	F0 (LRB)	250				0.0083	
		300				0.0094	
R60	F1	800	612			0.0480	1127

Table 3: Fire parameters in the EC1 time-temperature curve [8].

The corresponding EC1 time-temperature curves are shown in Figure 2, with reference to the F1 (Figure 2a) and F0 (Figure 2b) fire scenarios.

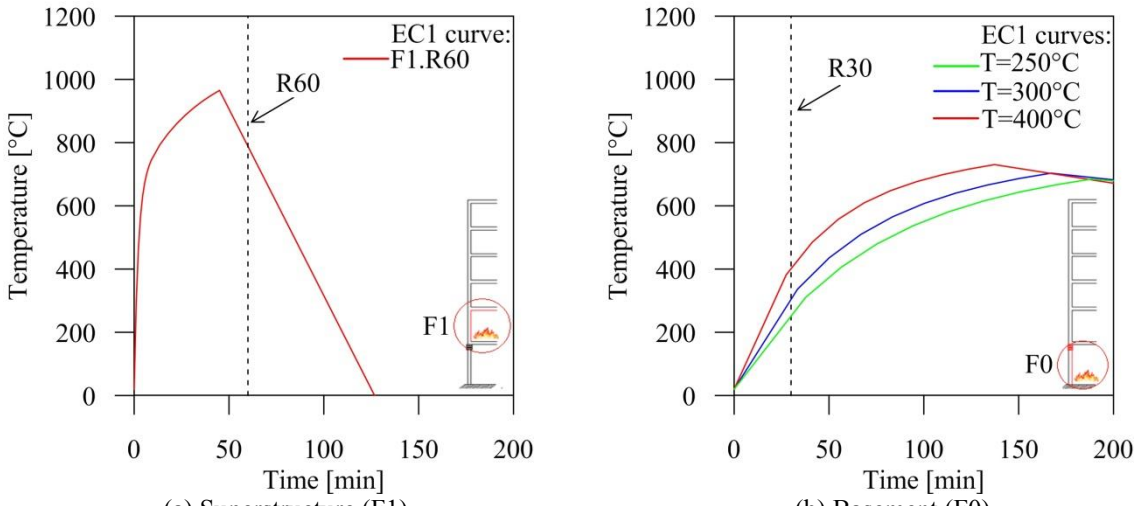

(a) Superstructure (F1). (b) Basement (F0).

Figure 2: Natural (EC1) fire curves for different fire scenarios [8].

As can be observed, temperatures corresponding to R30 in the basement are always placed in the heating branch of the time-temperature curves, unlike R60 in the superstructure characterized by a temperature in the cooling branch.

Once the time-temperature curve of the fire compartment is determined with the EC1 model, it becomes possible to evaluate the temperature distribution in the r.c. frame members and isolators, by means of the ABAQUS structural program [9]. Mean values of thermal parameters adopted for the structural materials in the finite element analysis are reported in Table 4: i.e. thermal conductivity, k; specific heat, c_p; density, ρ. On the assumption that the temperature does not change along the longitudinal axis, two-dimensional thermal mappings of cross-sections of the interior and perimeter r.c. frame members are shown in Figure 3, with reference to the first level of the superstructure (i.e. F1 and F0/1 fire scenarios) with R60 fire resistance. By contrast, three-dimensional plots need to be considered for the non-isotropic isolators, where mainly longitudinal (i.e. through steel shims) and much lower transversal (i.e. through layers of rubber) conduction takes place. To this end, isolators in the basement (i.e. F0 and F0/1 fire scenarios) with R30 fire resistance are represented in Figure 4, distinguishing HDLRB (see Figures 4a,b corresponding to T=300°C and 400°C, respectively) and LRB (see Figures 4c,d corresponding to T=250°C and 300°C, respectively).

Material	*k [W/mK]*	*c_p [J/kgK]*	*ρ [kg/m^3]*
Concrete	2	1000	2400
Rubber	0.17	1400	1200
Steel	50	450	7800
Lead	35	130	11300

Table 4: Thermal properties of the structural materials.

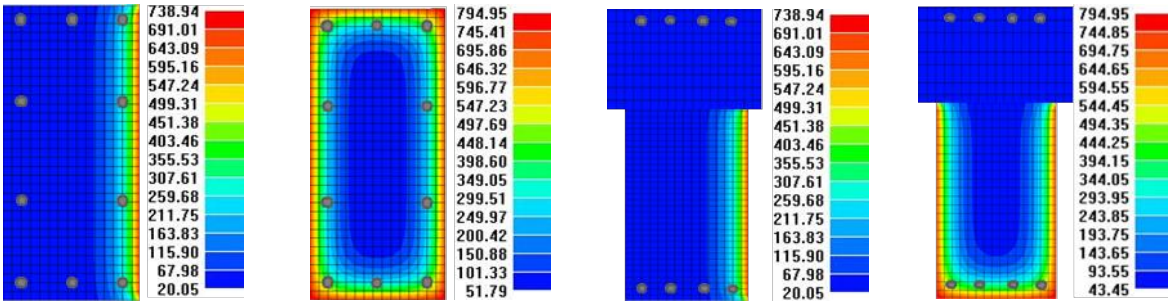

(a) Exterior column: t_{dc}=0.025m, corner bar, $f_{y,ds}$=445MPa, perimeter bar, $f_{y,ds}$ =438MPa

(b) Interior column: t_{dc}=0.035m, corner bar, $f_{y,ds}$=240MPa, perimeter bar, $f_{y,ds}$=434MPa

(c) Exterior beam: t_{dc}=0.025m, corner bar, $f_{y,ds}$=445MPa

(d) Interior beam: t_{dc}=0.035m, corner bar, $f_{y,ds}$=240MPa, perimeter bar, $f_{y,ds}$=428MPa

Figure 3: Two-dimensional thermal mappings for r.c. frame members (F1 and F0/1 fire scenarios, R60).

Thermal mapping of the r.c. cross-sections combined with the 500°C isotherm method proposed by Eurocode 2 [10] ignore concrete with temperatures exceeding 500°C. More specifically, on the fire-exposed sides of the cross-sections, the thickness of the damaged concrete (t_{dc}) and the reduced (damaged) yield strength ($f_{y,ds}$) of each corner and perimeter steel reinforcement, evaluated with respect to the temperature in the centre of the bar, are also reported in Figure 3. It is worth noting that some of the reinforcing bars may fall outside the reduced cross-section, but they are still included in the calculation of the ultimate values of strength and curvature ductility. Fire effects in the basement consist in a reduction of the seismic load capacity of HDLRBs and LRBs, which are subjected to irreversible degradation when exposed to high temperatures. However, vulcanization between layers of rubber and steel plates makes rubber more resistant to changes in temperature. Thus, a 200°C isotherm method is adopted [16], where rubber with temperatures exceeding the vulcanization

threshold is not considered, while the residual cross-section retains its initial values of strength and stiffness. In detail, the radial thickness of the damaged rubber (t_{dr}) on the fire-exposed cross-sections of HDLRBs and LRBs is also reported in Figures 4a,b and 4c,d, respectively.

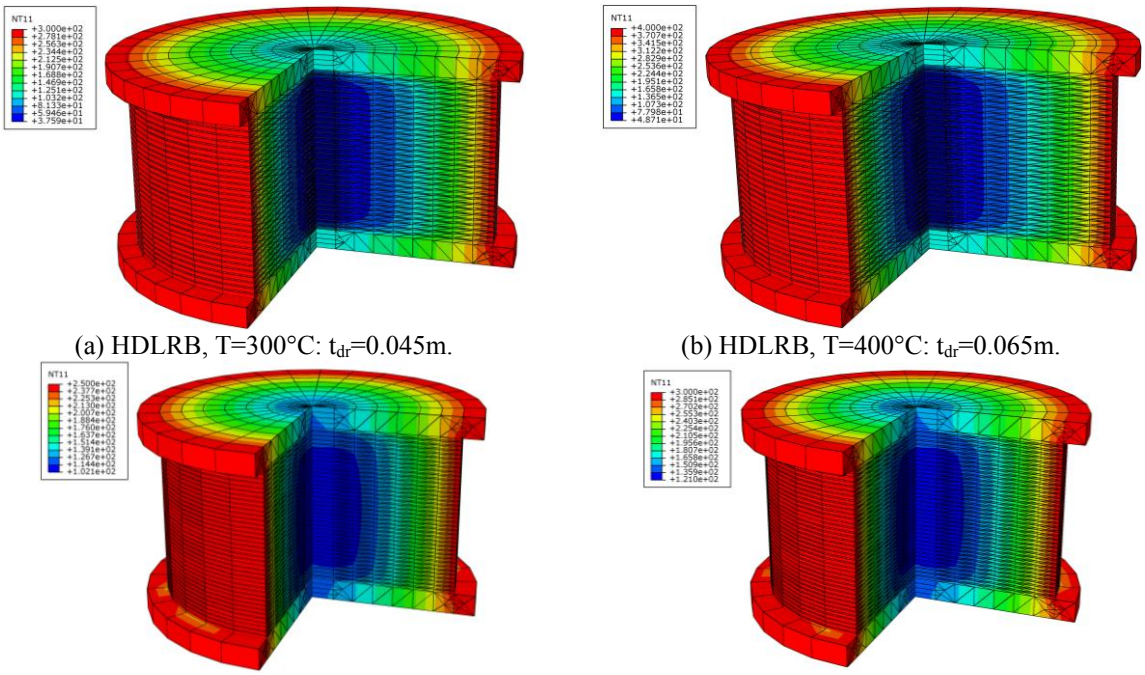

(a) HDLRB, T=300°C: t_{dr}=0.045m. (b) HDLRB, T=400°C: t_{dr}=0.065m.

(c) LRB, T=250°C: t_{dr}=0.034m. (d) LRB, T=300°C: t_{dr}=0.061m.

Figure 4: Three-dimensional thermal mappings for isolators (F0 and F0/1 fire scenarios, R30).

In Figure 5, reduction factors of the flexural stiffness $\alpha_{KF,T}(=K_{F,T}/K_{F,0})$ are plotted as function of the time of fire exposure for columns (Figure 5a) and beams (Figure 5b) in the first level, assuming a direct correspondence between the examined level and the fire compartment. As expected, interior columns and beams exposed to fire on four and three sides, respectively, highlight $\alpha_{KF,T}$ lower values than those obtained for exterior columns and beams exposed to fire on one side only.

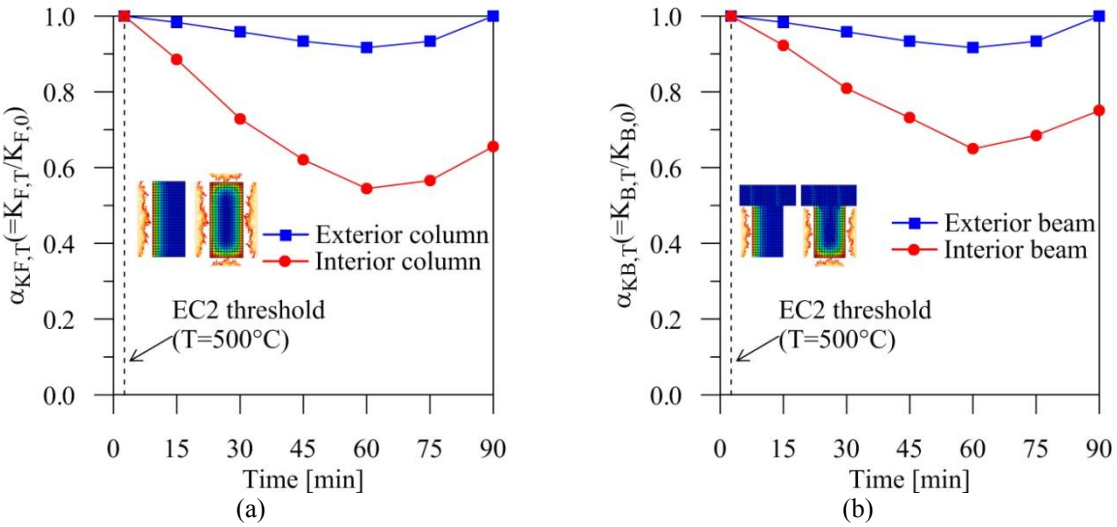

Figure 5: Reduction factors of flexural stiffness for r.c. frame member exposed to fire.

The time threshold corresponding to T=500°C is also plotted in Figure 5 as a reference value. Moreover, for all the examined cases, it is interesting to note that the minimum value of $\alpha_{KF,T}$ corresponds to R60 although, in accordance with EC1 natural fire curve shown in Figure 2a, the temperature profile shows a decrease during the cooling phase.

Next, reduction factors of the effective shear $\alpha_{KS,T}(=K_{S,T}/K_{S,0})$ and axial $\alpha_{KA,T}(=K_{A,T}/K_{A,0})$ stiffnesses and primary and secondary $\alpha_{S,T}(=S_T/S_0)$ shape factors are shown in Figure 6, as function of the fire temperature for HDLRBs (Figure 6a) and LRBs (Figure 6b) in the basement. The proposed temperature threshold (i.e. T=200°C) is also plotted as a reference value. As can be observed, reduction factors for LRBs are always higher than for HDLRBs, due to their lesser diameter. Moreover, the highest reduction factors are obtained for $\alpha_{KA,T}$ where the compression modulus also decreases for increasing values of fire temperature.

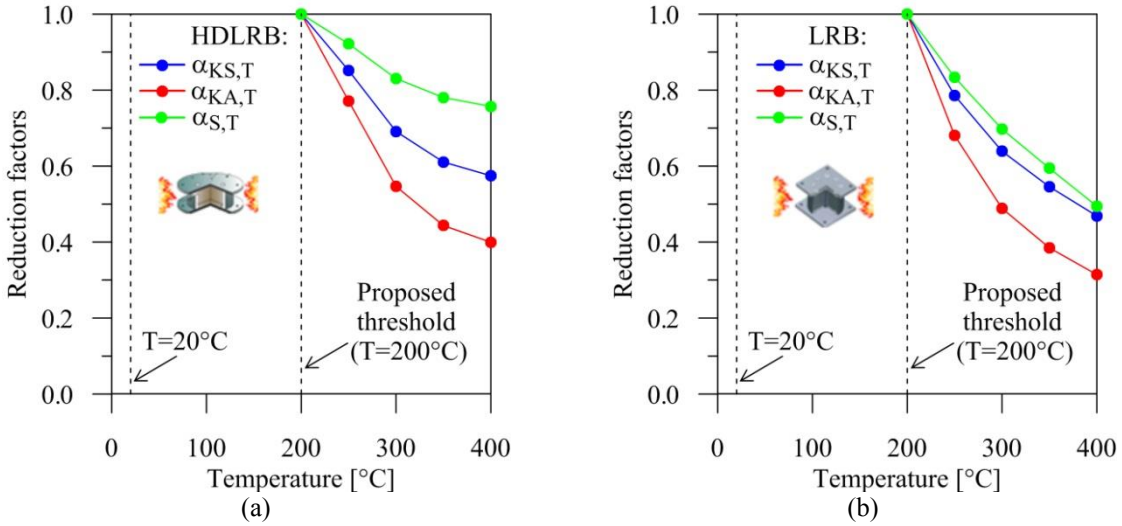

Figure 6: Reduction factors of mechanical and geometrical properties for isolators exposed to fire.

4 NEAR- AND FAR-FAULT EARTHQUAKES

To study the residual seismic load capacity of fire-damaged r.c. base-isolated buildings, the horizontal components of real near- and far-fault ground motions are considered in line with the design hypotheses adopted for the test structures: i.e. high-risk seismic zone and medium-dense subsoil type. In detail, seven near-fault earthquakes (NFE set), exhibiting high-amplitude and long-period velocity pulses [17], are selected from the Pacific Earthquake Engineering Research center database [11]. Next, seven far-fault earthquakes (FFE set), reflecting the provisions of the Italian seismic code [7, 18] for the geographical coordinates (longitude 17.08° and latitude 39.11°) at the site where the building is hypothesized, are derived by the European Strong Motion database [12]. In Tables 5 and 6, the main data of the NFE and FFE sets are reported, respectively: i.e. country, date, recording station, component, magnitude, peak ground acceleration. The corresponding elastic response spectra of velocity ($S_{v,H}$) are plotted in Figure 7, assuming an equivalent viscous damping ratio in the horizontal direction, ξ_H, equal to 5%. The response spectra are compared with the corresponding target NTC08 response spectra at the serviceability (i.e. operational, PGA_{OP}=0.108g) and ultimate (i.e. life-safety, PGA_{LS}=0.283g, and collapse prevention, PGA_{CP}=0.345g) limit states. As can be observed, spectral values of the selected near-fault (Figure 7a) and far-fault (Figure 7b) earthquakes are quite different from those corresponding to the NTC08 spectra, in the range of rather long vibration periods which are more significant for the base-isolated test structures, hence requiring evaluation of suitable scale factors. The selection of an intensity measure to

predict structural demand of base-isolated buildings is a difficult task, because ground motions characterized by similar spectral values at specific vibration periods can produce different structural responses due to the lengthening of vibration periods as the structure enters the inelastic range. In the present work, the *Modified Velocity Spectrum Intensity* (MVSI), obtained from integration of the velocity (elastic) response spectra over a defined range of vibration periods (T), is adopted [19-21]:

$$MVSI = \int_{0.5T}^{1.25T} S_{v,H}(T,\xi) \cdot dT \tag{5}$$

Then, the selected real accelerograms are normalized with respect to the NTC08 ones by scaling their PGA_H values

$$PGA_{H,S}^{NFE} = PGA_H^{NFE} \cdot SF_{NFE};\ PGA_{H,S}^{FFE} = PGA_H^{FFE} \cdot SF_{FFE} \tag{6a,b}$$

through the scale factors for NFE and FFE sets

$$SF_{NFE} = MVSI_{NTC08} / MVSI_{NFE};\ SF_{FFE} = MVSI_{NTC08} / MVSI_{FFE} \tag{7a,b}$$

Country	*Earthquake*	*Date*	*Station*	*Component*	M_w	PGA_H
Taiwan	Chi-Chi	20/09/1999	TCU068	EW	7.3	0.566 g
USA	Northridge	17/01/1994	Rinaldi	228	6.6	0.837 g
USA	Superstition Hills	24/11/1987	Parachute	225	6.4	0.455 g
USA	Cape Mendocino	25/04/1992	Petrolia	090	7.1	0.662 g
Japan	Kobe	16/01/1995	Takatori	090	6.9	0.616 g
Iran	Tabas	16/09/1978	Tabas	TR	7.7	0.852 g
Turkey	Erzincan	13/03/1992	Erzincan	NS	6.7	0.515 g

Table 5: Main data of the selected near-fault ground motions.

Country	*Earthquake*	*Date*	*Station*	*Component*	M_w	PGA_H
Greece	Alkion	24/02/1981	Korinthos-OTE Building	000333xa	6.6	0.230g
Turkey	Adana	27/06/1998	Ceyhan-Tarim Ilce	001726ya	6.3	0.270g
Italy	Friuli	15/09/1976	Buia	000151xa	6.0	0.083g
Italy	Umbria-Marche	26/09/1997	Castelnuovo-Assisi	000600ya	6.0	0.106g
Turkey	Izmit	13/09/1999	Adapazari Bayindirlik	006978ya	5.8	0.071g
Turkey	Ishakli	03/02/2002	Afyon-Bayindirlik	007104ya	5.8	0.052g
Turkey	Dinar	01/10/1995	Dinar-Meteoroloji	000879ya	6.4	0.319g

Table 6: Main data of the selected far-fault ground motions.

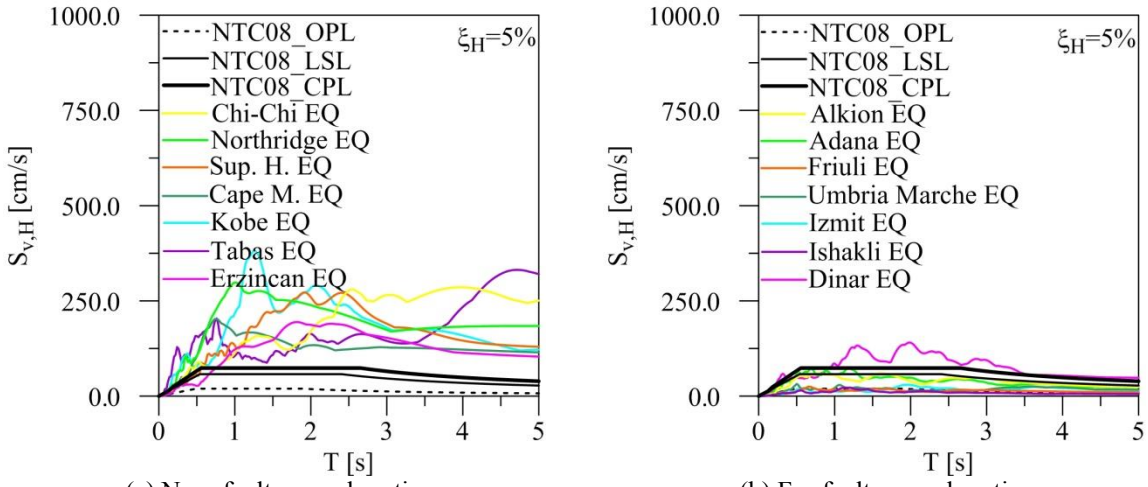

(a) Near-fault ground motions. (b) Far-fault ground motions.

Figure 7: Velocity (elastic) response spectra.

5 NUMERICAL RESULTS

A multi-record incremental dynamic analysis (IDA) of the base-isolated structures is carried out in a series of nonlinear dynamic analyses under the above mentioned NFE and FFE sets of seven near-fault and far-fault earthquakes, respectively. It should be noted that each earthquake is scaled to several intensity levels (a_g) of the corresponding PGA value, but all earthquakes are preliminarily normalized by scaling their PGA value with reference to the *Modified Velocity Spectrum Intensity* provided by NTC08 at the CP limit state. Afterwards, a mean of the results separately obtained for ground motions of the NFE and FFE sets is calculated. Specifically, the mean IDAs are interrupted once the ultimate state on the base-isolation systems and superstructure are reached. The ultimate values of the total shear strain ($\gamma_{tot,u}$) and the corresponding shear strain due to seismic displacement ($\gamma_{s,u}$) of the HDLRBs and LRBs are assumed equal to 1.5 times the corresponding design values. Moreover, the compressive and tensile axial loads of the HDLRBs and LRBs are limited to the critical buckling load and the ultimate tensile load, respectively. On the other hand, the local damage suffered by the r.c. frame members is evaluated by considering the ultimate ductility demand calculated in terms of curvature at the potential critical sections of the beams (i.e. end, quarter-span and mid-span sections) and columns (i.e. end sections). A two-spring-two-dashpot model is adopted for modelling the coupling of horizontal and vertical responses for HDLRBs [22]. Moreover, LRBs are idealized by means of a two-component model, comprising an elastic-perfectly-plastic component and an elastic component, based on a bilinear force-displacement law. Finally, a lumped plasticity model based on the Haar-Kàrmàn principle describes the elastic-plastic response of the r.c. frame members, assuming a bilinear moment-curvature law with hardening ratio equal to 3% [23]. In the present work, viscous damping in the isolation system is avoided by using the hysteretic models of the HDLRBs and LRBs, while the damping matrix of the superstructure is calculated on the basis of the Rayleigh damping, assuming constant values of the damping coefficients evaluated from the modal analysis of the base-isolated structure with the initial stiffness of the isolation system [24]. Specifically, a viscous damping ratio equal to 2% is considered with reference to the two vibration periods corresponding to high-participation modes with components prevailing in the horizontal (T_{IH}) or vertical (T_{IV}) direction, respectively.

To represent seismic effects in the fire-damaged basement, mean values of maximum total shear strain (γ_{tot}) and dimensionless axial load (P/P_{cr}) are plotted in Figure 8 for the HDLRBs (Figs. 8a,c) and LRBs (Figs. 8b,d), referring to base-isolated structures subjected to NFE and FFE sets of ground motions. The no fire condition is compared with the fire compartment in the basement at the end of 30 (i.e. R30) minutes of fire exposure. In particular, the F0A (i.e. T=300°C) and F0B (i.e. T=400°C) fire scenarios are considered for HDLRBs, while the F0C (i.e. T=250°C) and F0D (i.e. T=300°C) are examined for LRBs. Additionally, serviceability (i.e. operational limit, OPL) and ultimate (i.e. life-safety and collapse prevention limits, LSL and CPL) limit states are represented to highlight the probability of exceeding a specified limit-state given the a_g/PGA level. As can be observed, an amplification in the structural response of fire-exposed base-isolated structures is obtained for increasing values of fire temperature (T) and dimensionless acceleration ratio α_a(=a_g/PGA). This result is more pronounced for the NFE set (solid lines) than for the FFE set (dashed lines), confirming the detrimental effects of pulse-like near-fault ground motions on base-isolated structures. Moreover, the F0A and F0C scenarios correspond to fire temperatures generally reaching the CPL state for HDLRBs and LRBs, respectively. Under the NFE set of ground motions, the F0B scenario corresponds to collapse of the HDLRBs before reaching the LSL state (Figure 8a), while the F0D scenario is border-line for the LRBs (Figures 8b,d). However, the residual seismic load capacity of the

HDLRBs is greater than that observed for the LRBs, because the F0A and F0B scenarios correspond to a higher temperature than that obtained for the F0C and F0D scenarios, respectively. This result can be interpreted by observing that for a same value of fire temperature (e.g. T=300°C in the F0A and F0D scenarios) the percentage of the damaged rubber increases for decreasing values of the initial diameter of the isolator (see Table 2). Finally, maximum global ductility demand of the superstructure is plotted in Figures 8e and 8f referring to base-isolated structures with HDLRBs and LRBs, respectively. It is interesting to note that the no fire condition corresponds to the highest values of ductility demand for both NFE and FFE sets of ground motions, highlighting the fact that the elongation of the fundamental vibration period due to fire damage in the base-isolation system prevents high ductility demand in the superstructure.

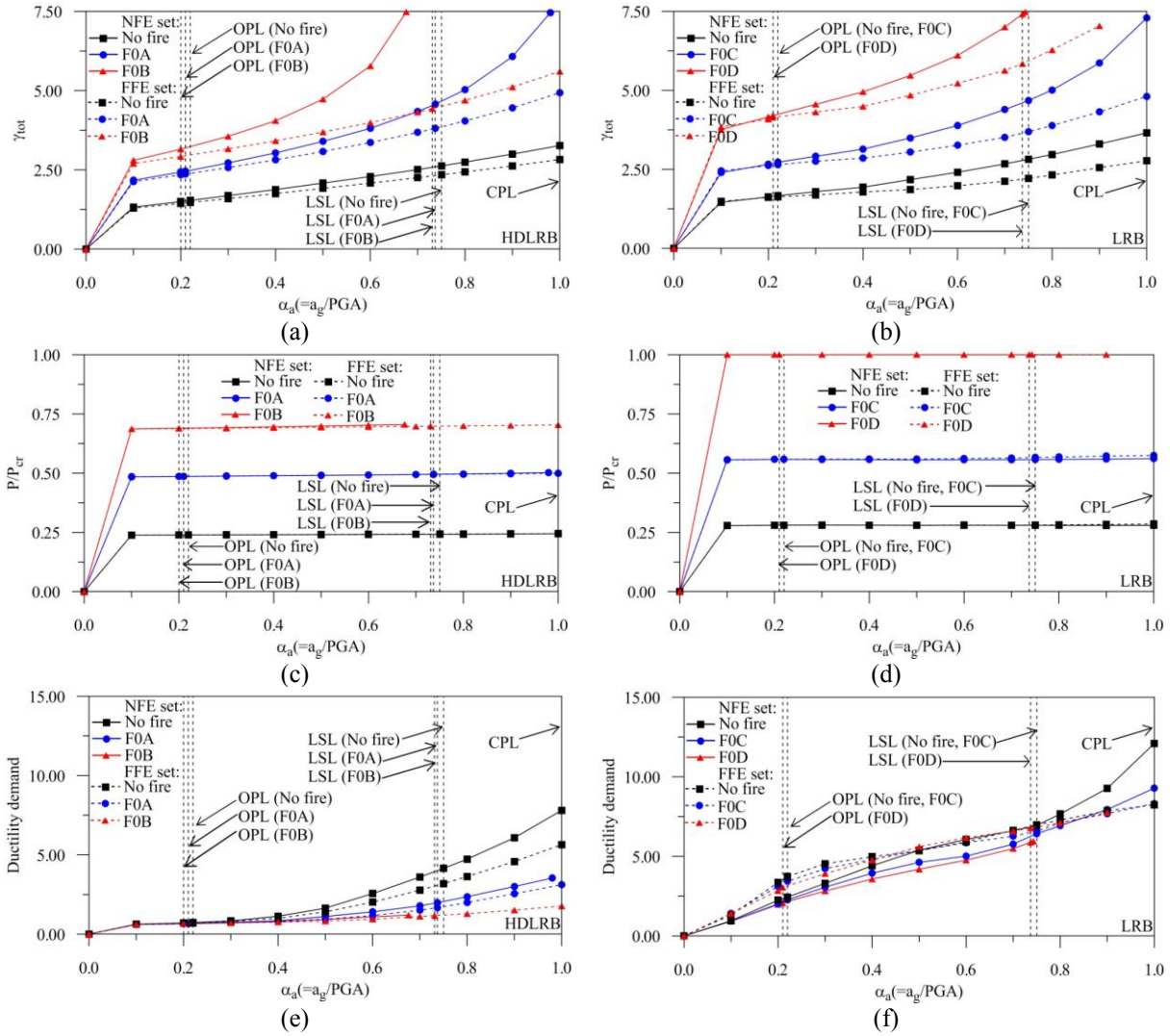

Figure 8: Nonlinear incremental dynamic analysis under near-fault (NFE set) and far-fault (FFE set) earthquakes: comparison of base-isolated structures in the no fire and fire scenarios.

Plots similar to the previous ones are reported in Figure 9 to illustrate seismic effects in the basement (Figures 9a-9d) and superstructure (Figures 9e,f), on the assumption that the fire compartment is only confined to the area of the first level (i.e. F1 scenario with fire resistance R60) or also occurs simultaneously in the basement (i.e. F0A/1 and F0C/1 scenarios). Specifically, the F0A/1 (Figures 9a,c,e) and F0C/1 (Figures 9b,d,f) scenarios are considered for the

HDLRBs and LRBs subjected to T=300°C and T=250°C fire temperatures, respectively. As can be observed, all base-isolated structures are able to reach the dimensionless acceleration ratios α_a related to the LSL and CPL states, for both the NFE and FFE sets of ground motions, the F0A/1 scenario being the only exception with γ_{tot} ultimate value for the HLDRBs corresponding to α_a=0.98 (Figure 9a). Similar responses of the base-isolation systems are obtained for the no fire and F1 scenario, for both HDLRBs (Figures 9a,c) and LRBs (Figures 9b,d), because the residual seismic load capacity of the base-isolated structures depends on fire damaged r.c. frame members in the first level of the superstructure. As expected, the post-fire seismic performance of the superstructure (Figures 9e,f) for the F1 fire scenario is worse than that of the base-isolated structure in the no fire condition and F0/1 fire scenarios. It is worth noting that the ductility demand of base-isolated structures equipped with LRBs mainly depends on the FFE set for low-intensity earthquakes (i.e. a_g/PGA<0.5) while it is more influenced by the NFE set for increasing values of a_g/PGA (Figure 9f). This behaviour can be interpreted by observing that the horizontal stiffness of the LRBs significantly increases at the small amplitude deformations, shortening the fundamental vibration period and consequently shifting the response towards the resonant region in the acceleration response spectrum of the FFE set.

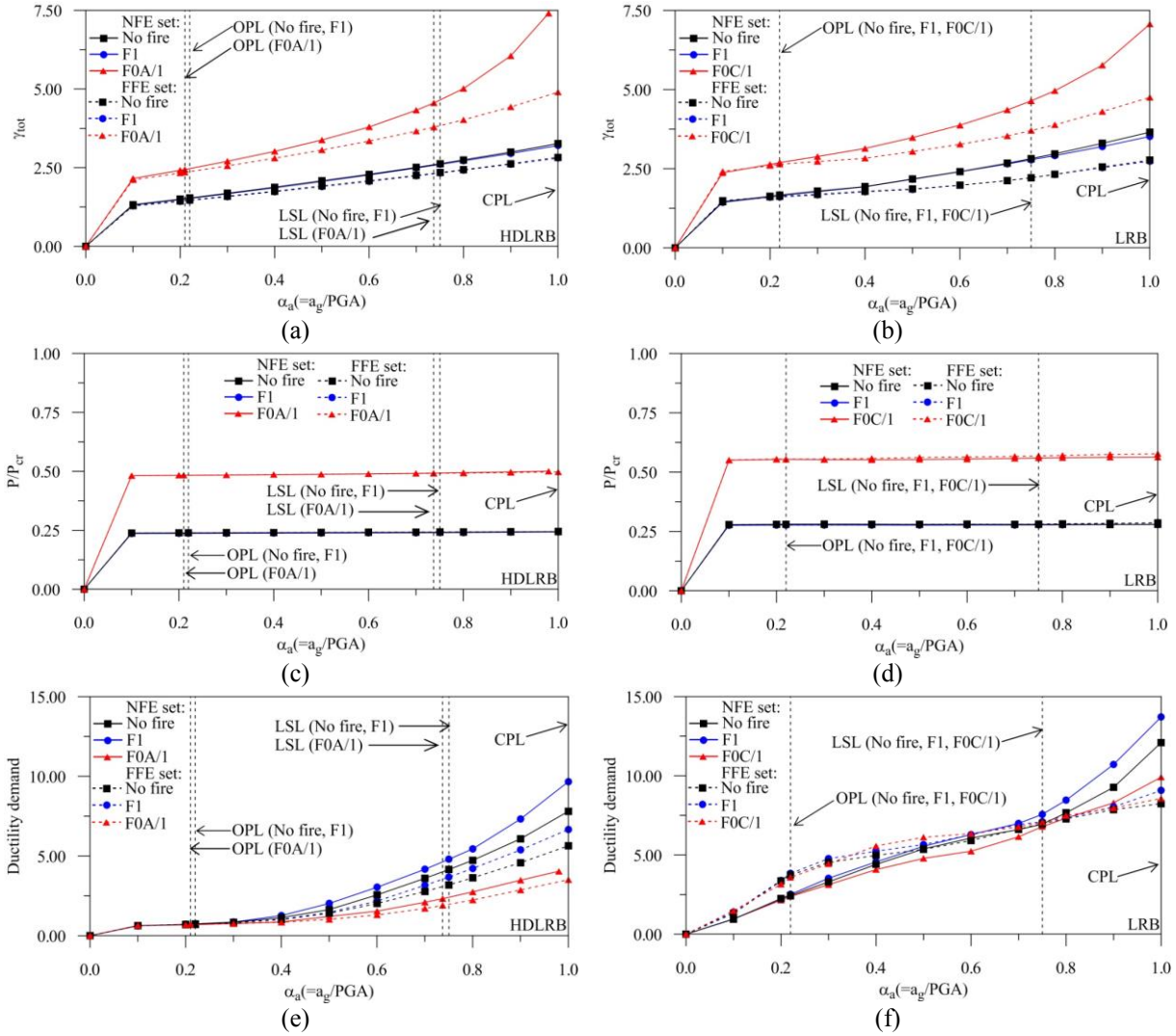

Figure 9: Nonlinear incremental dynamic analysis under near-fault (NFE set) and far-fault (FFE set) earthquakes: comparison of base-isolated structures in the no fire and fire scenarios.

To investigate the distribution of local damage along the building height, mean ductility demand at end sections of interior beams is plotted in Figure 10, considering base-isolated structures with HDLRBs (Figures 10a,c) and LRBs (Figures 10b,d) subjected to the NFE and FFE sets of earthquakes. A picture of the residual load capacity at the CPL state is generally represented, assuming the minimum value of the dimensionless acceleration ratio α_a for both NFE and FFE sets when the IDAs are early interrupted. In detail, this happens in the case of the F0A, F0B, F0D and F0A/1 scenarios, due to the attainment of the ultimate value imposed on the total shear strain of the isolators under the NFE set. The effects of the NFE set on the ductility demand are found to be more marked at the lower floors when the F1 fire scenario is considered (Figures 10c,d), while the no fire condition always prevails over the cases of fire occurring in the basement (i.e. F0 scenarios) and simultaneously in the first level of the super-structure (i.e. F0A/1 and F0C/1 scenarios). Moreover, the effects of the FFE set are generally more significant than those of the NFE set at the higher floor levels of base-isolated structures with LRBs (Figures 10b,d). Further results, omitted for the sake of brevity, confirm similar findings for the quarter-span sections of the interior beams while mid-span sections of beams together with end-sections of the columns exhibit negligible ductility demand.

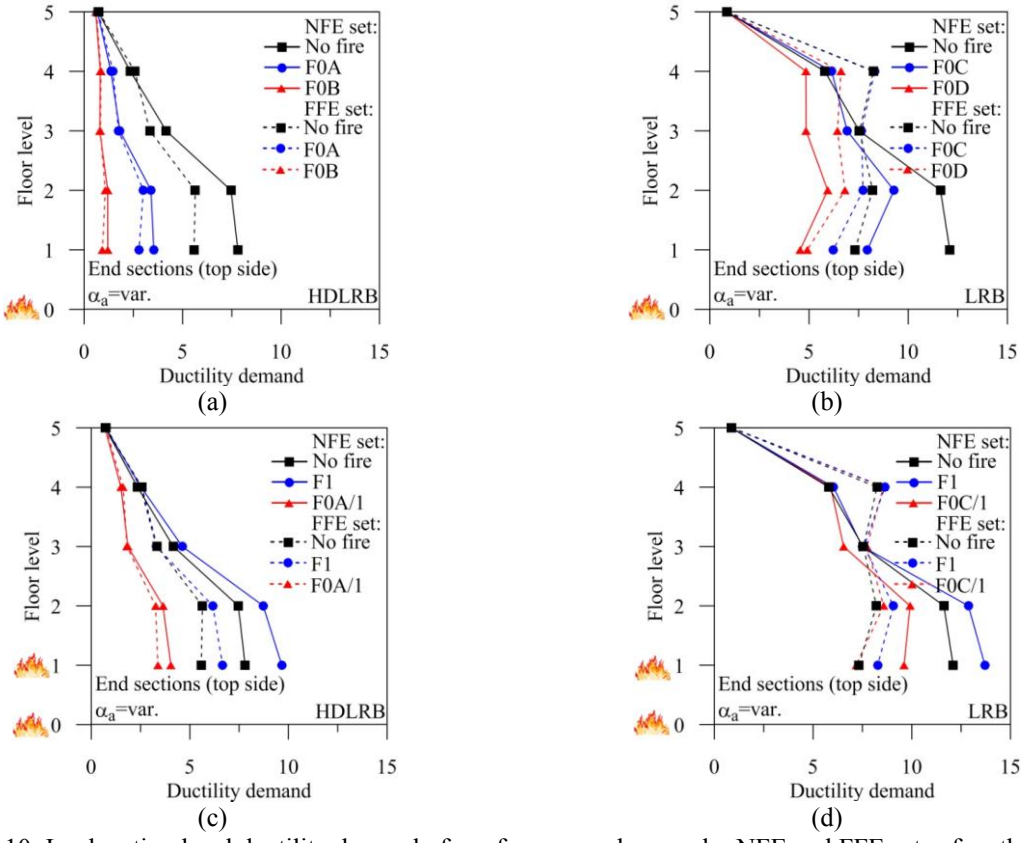

Figure 10: In-elevation local ductility demand of r.c. frame members under NFE and FFE sets of earthquakes: base-isolated structures with HDLRBs and LRBs.

Finally, the local in-plan damage distribution of the isolators is plotted in Figure 11, with reference to HDLRBs (Figures 11a,c) and LRBs (Figure 11b,d) of the base-isolated structures subjected to NFE and FFE sets of earthquakes. Only the fire scenarios in the basement are compared for the HDLRBs (i.e. F0A and F0B) and LRBs (i.e. F0C and F0D). Specifically, total shear strain (γ_{tot}) and dimensionless axial load (P/P_{cr}) are contemporaneously examined, by considering only half of the symmetric building plan. In all the examined cases, maximum values of γ_{tot} and P/P_{cr} under the NFE set are obtained for the central isolator followed by the

interior one. As expected, local response parameters of the isolators under the FFE set of earthquakes are generally lower than under the NFE set. Moreover, the effectiveness of the LRBs to retain a residual seismic load capacity is limited in comparison with the HDLRBs, also taking into account the lower temperatures (i.e. T=250°C and 300°C) characterizing the F0C and F0D fire scenarios with respect to F0A and F0B ones (i.e. T=300°C and 400°C).

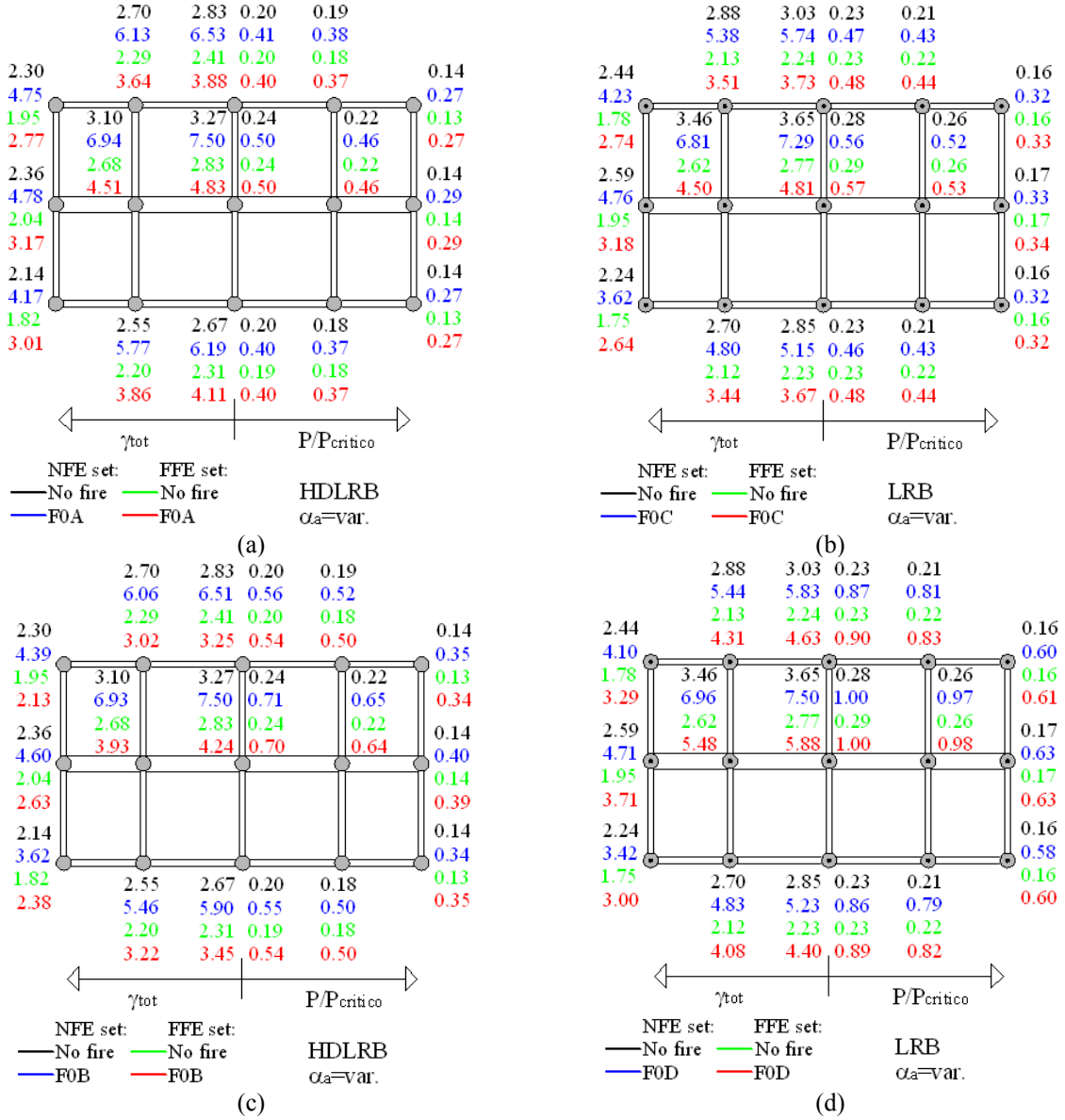

Figure 11: In-plan local response parameters of the isolators under NFE and FFE sets of earthquakes: base-isolated structures with HDLRBs and LRBs.

6 CONCLUSIONS

A multi-record nonlinear incremental dynamic analysis of base-isolated framed structures, damaged by fire and then subjected to near- and far-fault earthquakes, is carried out in order to evaluate their residual seismic load capacity. To this end, different scenarios are considered, involving fire in the first level of the superstructure and/or in the base-isolation system made with rubber bearings (i.e. HDLRBs and LRBs). To evaluate the temperature distribution in the r.c. frame members and isolators, bi- and three-dimensional thermal mappings are evaluated by means of the ABAQUS computer code. Similarly to the 500°C isotherm method proposed

by Eurocode 2 to evaluate residual properties of fire-damaged r.c. cross-sections, a 200°C isotherm method is proposed for the residual cross-section of HDLRBs and LRBs, neglecting rubber with temperatures exceeding the vulcanization threshold with steel shims. Fire loading before earthquake confirms reduction factors of the flexural stiffness for interior columns and beams exposed to fire on four and three sides, respectively, lower than those obtained for exterior columns and beams exposed to fire on one side only. Next, reduction factors of the effective shear and axial stiffnesses and primary and secondary shape factors for LRBs exhibit values higher than for HDLRBs, due to their lesser initial diameter.

Seismic aftershocks after fire highlight amplification in the structural response of fire-exposed base-isolated structures for the NFE set rather than FFE set of earthquakes, confirming the detrimental effects of pulse-like near-fault ground motions on base-isolated structures. Under the NFE set, the F0B fire scenario corresponds to collapse of the HDLRBs before the attainment of the LSL state, while the F0D fire scenario is border-line for the LRBs. However, the residual seismic load capacity of the HDLRBs is greater than that observed for the LRBs, because the F0A and F0B scenarios are characterized by higher temperatures than for the F0C and F0D scenarios, respectively. The post-fire seismic performance of the superstructure for the F1 fire scenario is worse than that observed in the no fire condition and F0/1 scenarios. Note that maximum ductility demand of base isolated structures equipped with LRBs mainly depends on the FFE set for low-intensity earthquakes, while it is more influenced by the NFE set for increasing values of the acceleration ratio. Finally, the effects of the NFE set on the ductility demand are found to be more marked at the lower floor levels when the F1 fire scenario is considered, while the effects of the FFE set are generally more significant than those of the NFE set at the higher floor levels of base-isolated structures with LRBs.

ACKNOWLEDGEMENTS

The present work was financed by Re.L.U.I.S. (Italian network of university laboratories of earthquake engineering), in accordance with “Convenzione D.P.C.–Re.L.U.I.S. 2017, PR6 line, Isolation and Dissipation”.

REFERENCES

[1] V.K.R. Kodur, M. Garlock, N. Iwankiw. Structures in fire: state-of-the-art, research and training needs, *Fire Technology*, **48**, 825-839, 2012.

[2] B. Behnam, H. Ronagh. Performance of reinforced concrete structures subjected to fire following earthquake. *European Journal of Environmental and Civil Engineering*, **17**(4), 270-292, 2013.

[3] V.K.R. Kodur, N.K. Raut, X.Y. Mao, W. Khaliq. Simplified approach for evaluating residual strength of fire-exposed reinforced concrete columns. *Materials and Structures* **46**, 2059-2075, 2013.

[4] F. Mazza. Seismic vulnerability and retrofitting by damped braces of fire-damaged r.c. framed buildings. *Engineering Structures*, **101**, 179-192, 2015.

[5] F. Mazza. Effects of near-fault vertical earthquakes on the nonlinear incremental response of r.c. base-isolated structures exposed to fire. *Bulletin of Earthquake Engineering* **14**, 433-454, 2016.

[6] A.K. Bhowmick, R. Mukhopadhyah, S.K. De. High temperature vulcanization of elastomers. *Rubber Chemistry and Technology*, **52**(4), 725-734, 1979.

[7] NTC08. Technical Regulations for the Constructions. Italian Ministry of the Infrastructures, 2008.

[8] Eurocode 1. Actions on structures – Part 1-2: General actions, actions on structures exposed to fire. *C.E.N., European Committee for Standardization*, October 2004.

[9] ABAQUS. Computer software, Dassault Systems, version 6.12. Users and Theory Manual Version 6.12. Hibbitt, Karlsonn and Sorensen.

[10] Eurocode 2. Design of concrete structures – Part 1-2: General rules, structural fire design. *C.E.N., European Committee for Standardization*, December 2004.

[11] PEER. Pacific Earthquake Engineering Research Center database. http://peer.berkeley.edu/smcat/search.html, 2014.

[12] ESD. European Strong Motion database. http://esm.mi.ingv.it/, 2015.

[13] F. Mazza. Torsional response of fire-damaged base-isolated buildings with elastomeric bearings subjected to near-fault earthquakes. *Bulletin of Earthquake Engineering*, DOI 10.1007/s10518-017-0103-0, 2017.

[14] F. Mazza. Nonlinear incremental analysis of fire-damaged r.c. base-isolated structures subjected to near-fault ground motions. *Soil Dynamics and Earthquake Engineering*, **77**, 192-202, 2015.

[15] J. Weisman, G.P. Warn. Stability of elastomeric and lead-rubber seismic isolation bearings. *Journal of Structural Engineering*, **138**(2), 215-223, 2012.

[16] F. Mazza. Behaviour during seismic aftershocks of r.c. base-isolated framed structure with fire-induced damage. *Engineering Structures*, DOI10.1016/j.engstruct.2017.03.008.

[17] E. Chioccarelli, I. Iervolino. Near-source seismic demand and pulse-like records: A discussion for L'Aquila earthquake. *Earthquake Engineering and Structural Dynamics*, **39**(9), 1039-1062, 2010.

[18] I. Iervolino, C. Galasso, E. Cosenza. REXEL: computer aided record selection for code-based seismic structural analysis. *Bulletin of Earthquake Engineering,* **8**(2), 339-362, 2010.

[19] F. Mollaioli, A. Lucchini, Y. Cheng, G. Monti. Intensity measures for the seismic response prediction of base-isolated buildings. *Bulletin of Earthquake Engineering*, **11**: 1841-1866, 2013.

[20] F. Mazza, F. Alesina. Effects of site condition in near-fault area on the nonlinear response of fire-damaged base-isolated structures. *Engineering Structures*, **111**(3), 297-311, 2016.

[21] F. Mazza, R. Labernarda. Structural and non-structural intensity measures for the assessment of base-isolated structures subjected to pulse-like near-fault earthquakes. Soil Dynamics and Earthquake Engineering, **96**, 115-127, 2017.

[22] F. Mazza, A. Vulcano, Effects of the near-fault ground motions on the nonlinear dynamic response of base-isolated r.c. framed buildings. *Earthquake Engineering and Structural Dynamics*, **41**, 211-232, 2012.

[23] F. Mazza, M. Mazza, Nonlinear analysis of spatial framed structures by a lumped plasticity model based on the Haar-Kàrmàn principle. *Computational Mechanics*, **45**, 647-664, 2010.

[24] D.R. Pant, A.C. Wijeyewickrema, M.A. ElGawady. Appropriate viscous damping for nonlinear time-history analysis of base-isolated reinforced concrete buildings. *Earthquake Engineering and Structural Dynamics*, **42**, 2321-2339, 2013.